Article

Projected poleward migration of the Southern Ocean CO$_2$ sink region under high emissions

Check for updates

Precious Mongwe [1] ✉, Luke Gregor [2], Jerry Tjiputra [3], Judith Hauck[4], Takamitsu Ito [5], Christopher Danek[4], Marcello Vichi [6,7], Sandy Thomalla [1] & Pedro M. S. Monteiro[8]

The Southern Ocean is a major region of ocean carbon uptake, but its future changes remain uncertain under climate change. Here we show the projected shift in the Southern Ocean CO$_2$ sink using a suite of Earth System Models, revealing changes in the mechanism, position and seasonality of the carbon uptake. The region of dominant CO$_2$ uptake shifts from the Subtropical to the Antarctic region under the high-emission scenario. The warming-driven sea-ice melt, increased ocean stratification, mixed layer shoaling, and a weaker vertical carbon gradient is projected to together reduce the winter de-gassing in the future, which will trigger the switch from mixing-driven outgassing to solubility-driven uptake in the Antarctic region during the winter season. The future Southern Ocean carbon sink will be poleward-shifted, operating in a hybrid mode between biologically-driven summertime and solubility-driven wintertime uptake with further amplification of biologically-driven uptake due to the increasing Revelle Factor.

The Southern Ocean (south of 30°S) takes up approximately 40% of ocean anthropogenic CO$_2$ and ~75% of excess heat[1–4], making it one of the most pivotal ocean buffer of climate change. In addition, it supplies 33 – 75% of the nutrients required for new primary production in the global oceans[5–7]. Nevertheless, existing model projections indicate large uncertainty in the future Southern Ocean sink of anthropogenic CO$_2$ emissions[8]. In recent years, emergent constraints have shown some success in constraining uncertainty in the Southern Ocean CO$_2$ sink projections[8,9], nevertheless, changes in future mechanisms remain poorly understood. Understanding how climate change alters the Southern Ocean's ability to regulate CO$_2$ and heat exchanges, and their governing mechanisms is crucial to strengthening our confidence in the simulated future changes. Further, improved process understanding of the behavior of the Southern Ocean under extreme conditions like the high-emission scenario is essential to anticipate related ecosystems impacts and climate feedbacks in the future.

The intergovernmental panel on climate (IPCC) high emission-scenario projects over 1000 ppm atmospheric CO$_2$ (~ 2.5-factor increase) and associated warming of up to 4.5 °C by 2100 in the global ocean surface relative to the contemporary climate[10,11]. Simulated ocean related changes include, but are not limited to, sea-ice loss, ocean acidification, deoxygenation, and a decrease in CO$_2$ buffer capacity[12–17]. These predicted changes are key drivers to biogeochemical, ecosystems and physical ocean related gradual and abrupt regime shifts in projections. The decrease of the CO$_2$ buffering capacity for example is projected to enhance biological-induced CO$_2$ uptake in summer, and amplify the seasonal cycle of air-sea CO$_2$ fluxes (FCO$_2$) as well as acidification both of which may have a significant implications for the efficiency of the ocean CO$_2$ uptake and marine calcifying organisms in the Southern Ocean[18].

In this study, we investigate how these projected anthropogenically-driven changes will impact the magnitude and mechanisms of the Southern Ocean CO$_2$ uptake between the contemporary and the last decades of the 21st Century. We use nine state-of-art Earth System Models (ESMs) focusing on the historical and future high emission (SSP5-8.5) scenarios. The Southern Ocean is defined here as the region south of 30 °S, divided into three subdomains using dynamical frontal boundaries to reflect the three regimes of the Southern Ocean (Fig. 1). Namely, (i) the Subtropical region,

[1]Southern Ocean Carbon Climate Observatory (SOCCO), CSIR, Cape Town, South Africa. [2]Environmental Physics, Institute of Biogeochemistry and Pollutant Dynamics, ETH Zurich, Zurich, Switzerland. [3]NORCE Norwegian Research Centre, Bjerknes Centre for Climate Research, Bergen, Norway. [4]Alfred-Wegener-Institut, Helmholtz Zentrum für Polar- und Meeresforschung, Bremerhaven, Germany. [5]Earth and Atmospheric Sciences, Georgia Institute of Technology, Atlanta, GA, USA. [6]Department of Oceanography, University of Cape Town, Cape Town, South Africa. [7]Marine and Antarctic Research Centre for Innovation and Sustainability, University of Cape Town, Cape Town, South Africa. [8]School for Climate Studies, Stellenbosch University, Stellenbosch, South Africa. ✉e-mail: pmongwe@csir.co.za

Fig. 1 | Contemporary air-sea CO₂ flux (FCO₂) in the Southern Ocean. Obtained from **a** the ensemble mean of six pCO₂ products and **c** nine CMIP6 ESMs for the historical period (1995–2014), and **b, d** their variability computed as one standard deviation. FCO₂ is given gC m⁻² yr⁻¹ in all panels. Negative values indicate a flux into the ocean. The fronts are defined according to Orsi et al.[76] as black lines with the Subtropical Front to the North and the Polar Front to the South. The zones are defined as the subtropical region north of the Subtropical Front (outer line) to 30ºS, the Sub-Antarctic region between the two fronts, and the Antarctic region to the south of the Polar Front (inner line). Individual models are shown in Fig. Supplementary Fig. 7.
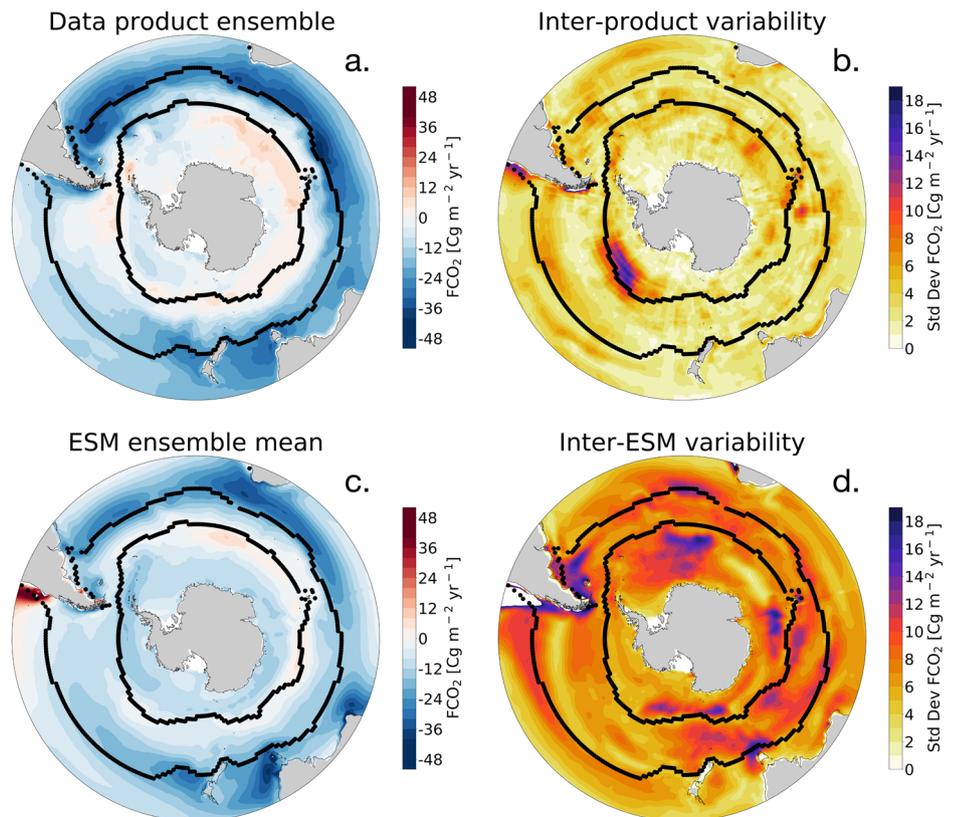
the warmest and most stratified part of the Southern Ocean, north of the Subtropical Front, (ii) the Sub-Antarctic region, a highly productive, moderately warm region that hosts the subduction of Subantarctic Mode and Antarctic Intermediate Waters, located between the Subtropical Front and the Polar Front; and (iii) the Antarctic region, south of the Polar Front, is characterized by the seasonal sea-ice cover, which regulates seasonal upwelling and primary production.

Results

Air-sea CO₂ flux mean state change between present and future climate

Observation-based, pCO₂-products annual mean air-sea CO₂ fluxes in the Southern Ocean are characterized by a strong CO₂ uptake within and north of the Subtropical Front (Subtropical region), a weak ingassing flux between the Subtropical and Polar Front (Sub-Antarctic region) and a weak out-gassing flux south of the Polar Front (Antarctic region), (Fig. 1a, see Methods for description and data available at Supplementary Data 1). ESMs broadly show good spatial agreement with the pCO₂-products ensemble north of the Subtropical Front (present climate 1995–2014, Fig. 1c). Differences between ESMs and pCO₂-products in the Subtropics mainly occur in the eastern Pacific, where most of the ESMs show a CO₂ outgassing feature. ESMs annual means are also comparable, overlapping within the envelope of the model spread with the pCO₂-products ensemble in the Subtropics; -15.5 ± 2.4 gC m⁻² yr⁻¹ (ESMs) and -16.4 ± 1.1 gC m⁻² yr⁻¹ (pCO₂-products), (Fig. 2a). In the Sub-Antarctic region, ESMs display a relatively larger model spread in comparison to the Subtropics, showing the largest disagreement in Malvina's sea (> 10 gC m⁻² yr⁻¹) and south of Australia (~ 9-10 gC m⁻² yr⁻¹). The ESMs ensemble mean (-9.0 ± 4.5 gC m⁻² yr⁻¹) for the Sub-Antarctic is nonetheless comparable to the observationally-derived pCO₂-products ensemble mean (-11 ± 0.8 gC m⁻² yr⁻¹) (Fig. 2b). The Antarctic region shows a comparable model spread with the Sub-Antarctic but does not overlap with the pCO₂-products. The Antarctic region is the weakest CO₂ sink of the three subdomains in the contemporary Southern Ocean, showing an annual mean

air-sea CO₂ flux (FCO₂) of -8.4 ± 5.4 gC m⁻² yr⁻¹ in ESMs and -1.81 ± 1.5 gC m⁻² yr⁻¹ in pCO₂-products (Fig. 2c).

At the end of the 21st century (2080–2099) a remarkably consistent pattern emerges in the ocean carbon uptake across ESMs; the region of the weakest CO₂ sink in the contemporary climate becomes the most intense sink. Namely, the region of the strongest CO₂ sink shift poleward from the Subtropics to the Antarctic (Fig. 2a–c). By the end of the 21st century, Subtropics contributes only about 23% (-22.0 ± 2.5 gC m⁻² yr⁻¹) of total Southern Ocean CO₂ uptake under the high-warming scenario in comparison to 47% in the contemporary climate. The CO₂ sink in the Subtropics increase by the smallest margin (6.6 ± 1.1 gC m⁻² yr⁻¹) in comparison of other Southern Ocean subdomains. The Sub-Antarctic region contributes 29% (-27.7 ± 5.4 gC m⁻² yr⁻¹) to the projected future, which is comparable to 27% in the present climate. The Antarctic region on the other hand displays the most extensive CO₂ sink increase of about 450% (-37.9 ± 7.3 gC m⁻² yr⁻¹), becoming the largest CO₂ sink region (48%) at the end of the 21st century (Figs. 1–2). The Antarctic region also has the largest annual mean FCO₂ model spread in the projected climate (Fig. 2c).

Mechanisms of air-sea CO₂ fluxes in the present climate

Air-sea CO₂ fluxes (FCO₂) are regulated by the thermodynamic and kine-matic forcings[19]. The thermodynamic forcing, the air-sea pCO₂ gradient (ΔpCO₂), is considered the primary driver of FCO₂; it determines the direction of the flux[20]. The kinematic forcing, on the other hand, controls the efficiency of gas transfer, and it is principally regulated by near-surface wind speeds. We note that kinematic forcing can induce indirect effects on the surface pCO₂, e.g., through changing the ocean circulation or water mass ventilation patterns[21]. On short timescales (hourly to weekly), kinematic forcing can also determine the magnitude and direction of FCO₂[22–25]. However, ΔpCO₂ plays a leading role in seasonal-scale FCO₂ variability[26,27]. Therefore, mechanisms regulating FCO₂ variability can be estimated from processes regulating ΔpCO₂. Further, considering that atmospheric pCO₂ is
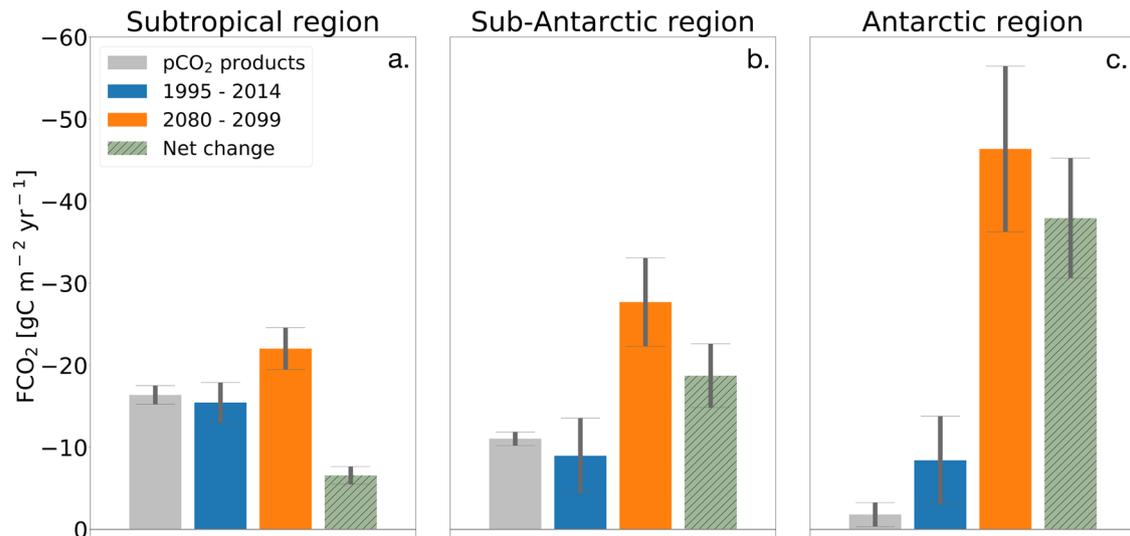
Fig. 2 | Present climate vs. end of the 21st century air-sea CO₂ fluxes in the Southern Ocean. a The Subtropical region on the right, **b** the Sub-Antarctic in the middle, and **c** Antarctic region on the left panel for the ensemble mean from nine CMIP6 ESMs, and the ensemble mean of six pCO₂ products for the historical period (1995–2015, blue and gray), and end of the 21st century (2080–2099, orange). The error bars reflect one standard deviation of the inter-model (product) spread. Individual models are shown in Supplementary Fig. 8.
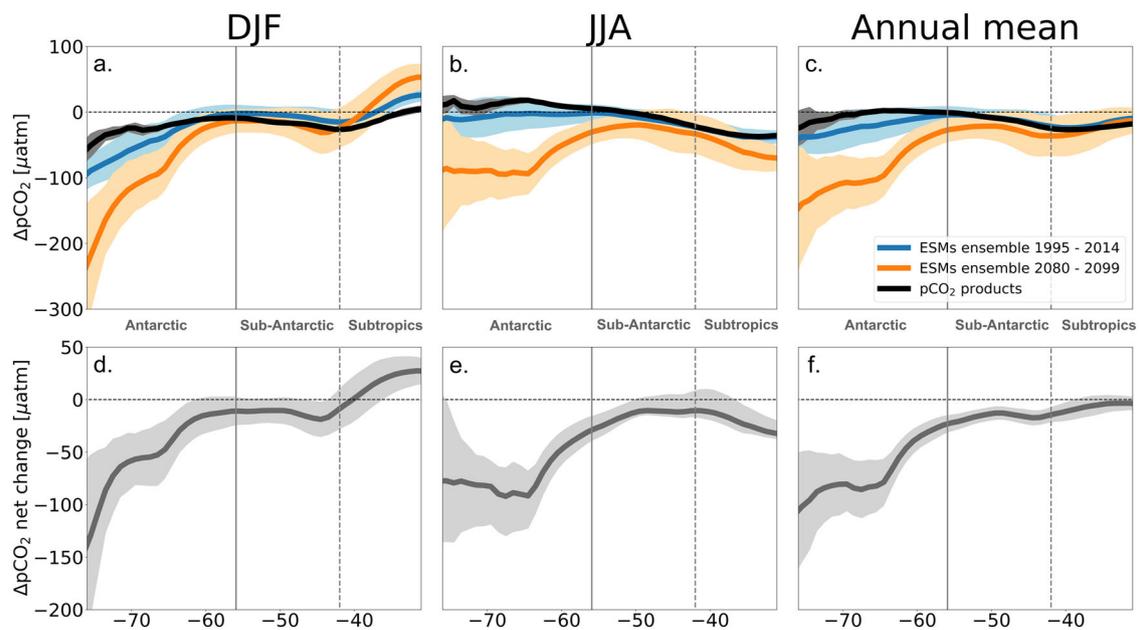

Fig. 3 | Seasonal and annual mean zonally averaged delta air-sea pCO₂ (ΔpCO₂) in the Southern Ocean. a–c from the ensemble mean of six pCO₂ products and nine CMIP6 ESMs for the present climate (blue line) and the end of the century (2080–2099, orange). **d–f** Net changes in the projected future climate (note the change of scale). The first, second, and third columns depict the austral summer (DJF), austral winter (JJA) averages, and the annual mean, respectively. The vertical gray lines denote the frontal positions, the solid line the Polar Front, and dotted the Subtropical Front. The shading in all figures shows the uncertainty; inter-model one standard deviation. Individual models are shown in Supplementary Fig. 9.

almost uniform in the Southern Ocean, ΔpCO₂ is ultimately controlled by the ocean pCO₂. Indeed, observed and ESMs ΔpCO₂ properties broadly delineate a similar latitudinal structure with FCO₂ (Figs. 2 and 3), showing a strong annual mean CO₂ ingassing flux in the Subtropics consistent with negative ΔpCO₂ (~-40 µatm) and decreasing poleward; > -30 µatm in the Sub-Antarctic, and near-zero value in the Antarctic region (Fig. 3a–c). Given that ESMs mean state magnitudes differ for some variables (e.g. pCO₂ and dissolved inorganic carbon (DIC) among others), comparing a multi-model seasonality is often impractical. Henceforth, we instead use monthly rates of change (first-order temporal derivatives, see Methods) for selected variables to highlight the changes in model and observed features at the seasonal scale.

Surface ocean pCO₂ and ΔpCO₂ variability is controlled by the relative contribution of thermal and nonthermal components[28,29]. The thermal component can empirically be estimated using the Takahashi et al.[30] formulation[30], and we estimate the nonthermal component by subtracting the thermal component from the total (Fig. 4, see Methods). The thermal component is driven by temperature variations through changes in gas solubility (Henry's law). The nonthermal component is mainly controlled by mixing and biology[31], it also includes the role of total alkalinity and
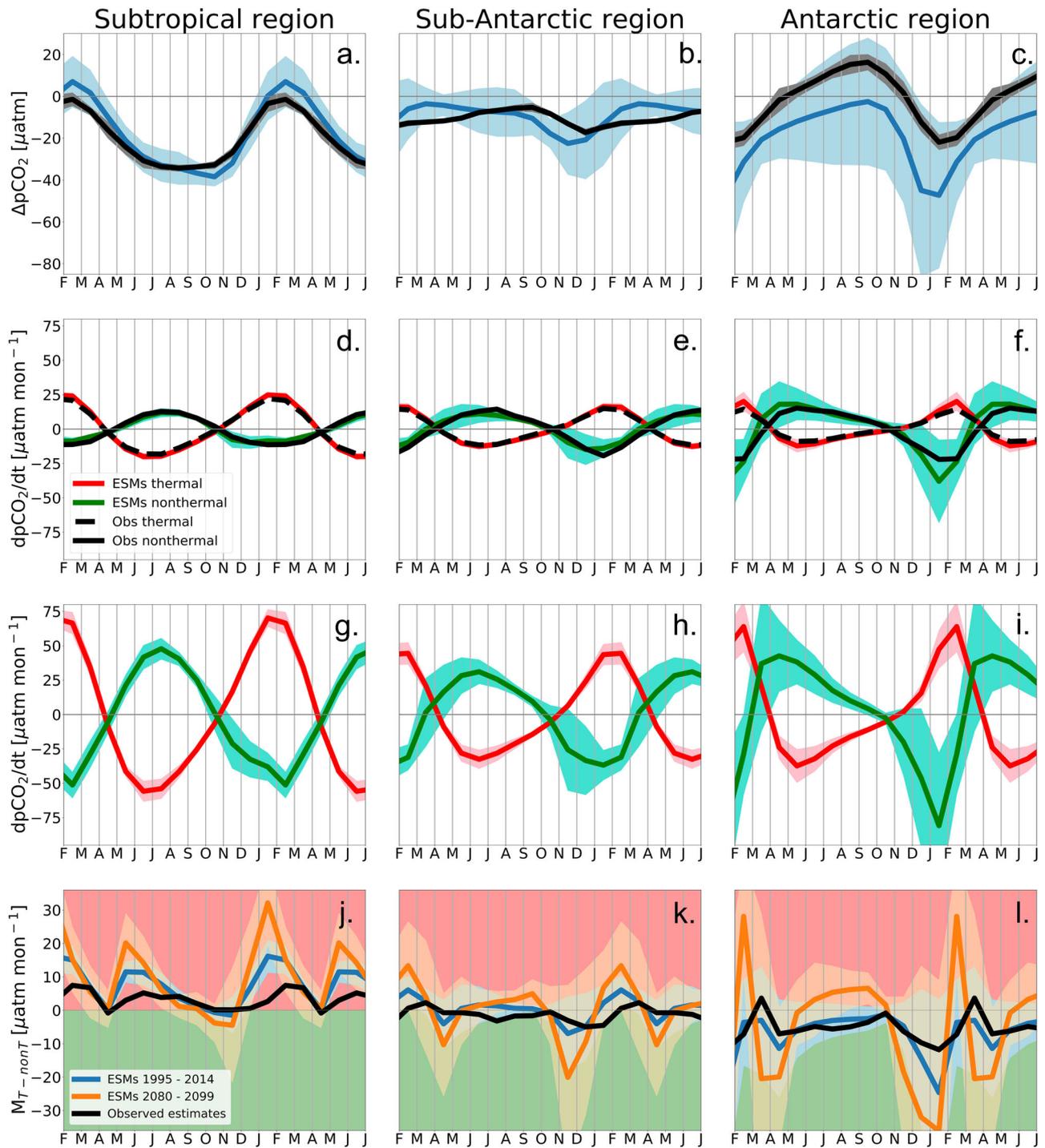
Fig. 4 | The seasonal cycle of delta air-sea pCO$_2$ (ΔpCO$_2$) and drivers of surface pCO$_2$ in the Southern Ocean. a–c The seasonal cycle of ΔpCO$_2$ for the ensemble model mean in blue and pCO$_2$-products in black. **d–i** seasonal cycle of the thermal and nonthermal components of pCO$_2$ changes for present climate **d–f** and the end of the 21st century **g–i. j–l** Seasonal cycle of thermal-nonthermal regimes from the metrics M$_{T-nonT}$ (Eq. 4, Methods). M$_{T-nonT}$ > 0 atm mon^{-1} denotes periods where the thermal component is leading monthly pCO$_2$ changes, while M$_{T-nonT}$ < 0 atm mon^{-1}, denotes dominance of nonthermal processes (biological and mixing). The shading in all figures shows the inter-modal variability, computed as the standard deviation. Individual models are shown in Supplementary Fig. 10.

salinity changes. However, total alkalinity and salinity have been shown to play a minor role in the seasonal cycle of ocean pCO$_2$ in the contemporary Southern Ocean[29,31], thus, here we focus on processes responsible for sources and sinks of DIC, i.e., primary production, respiration, and changes in seasonal mixing. The thermal and nonthermal components oppose each other on a seasonal scale[32,33] (Fig. 4d–f), and hence the larger of the two determines the observed seasonal cycle phasing of pCO$_2$, and ultimately

FCO$_2$[29]. The relative contributions of thermal and nonthermal components are assessed here through a metrics that calculates the absolute difference in their monthly rates (M$_{T-nonT}$, Eqs. 1–3, Methods). M$_{T-nonT}$ > 0 µatm mon^{-1} (Fig. 4j–l) denotes periods where (and when) the thermal component has a stronger influence on monthly pCO$_2$ changes than nonthermal processes (mixing and biology), and vice versa for M$_{T-nonT}$ < 0 atm mon^{-1}. For the contemporary climate, the observed ΔpCO$_2$ seasonality in the Subtropics is

Fig. 5 | The seasonal cycle of the physical and biological drivers of surface pCO₂. Seasonal cycle of **a**, **b** net primary production in the surface ocean (NPP) and **c**, **d** mixed layer depth (MLD), monthly rates of change of **e**, **f** surface dissolved inorganic carbon (dDIC/dt), **g**, **h** apparent oxygen utilization rate (dAOU/dt, **g**, **h**), and **i**, **j** surface temperature (dSST/dt) in the Sub-Antarctic region (left) and the Antarctic region (right). The blue lines are the present climate (1995–2014) and the orange lines are the end of the 21st century (2080–2099). Black lines depict observational estimates. The shading in all figures shows the inter-model standard deviation.
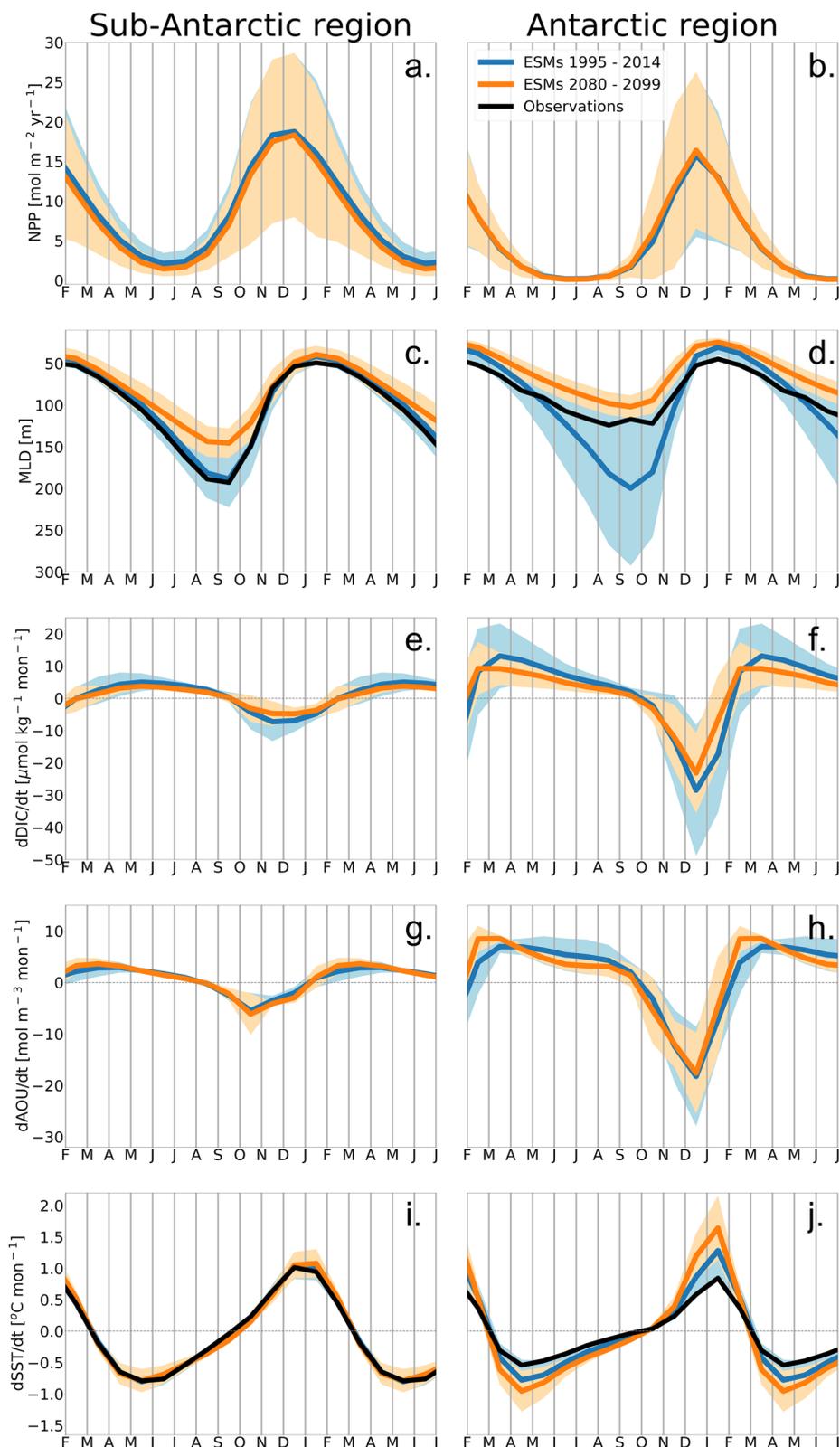
broadly controlled by thermal processes, has a near-equal contribution of the two components in the Sub-Antarctic, and is predominantly non-thermally controlled in the Antarctic region (Fig. 4a–c & j–l). ESMs broadly display good inter-model agreement in M_{T-nonT} with respect to the observed estimates in the Subtropics but show a degrading comparability poleward (Fig. 4d–l). Thermal constraints on CO_2 solubility that regulate the seasonal

cycle of pCO₂ in the Subtropics are as follows: negative ΔpCO₂ magnitudes in the autumn-winter seasons are due to higher gas solubility in cooler seasons, while the opposite is true in warmer seasons (Fig. 4a, d). The strong thermal dominance in Subtropics is partly because the largest seasonal temperature contrast (summer-winter difference) in the Southern Ocean occurs in the northern edge and decreasing poleward (Supplementary
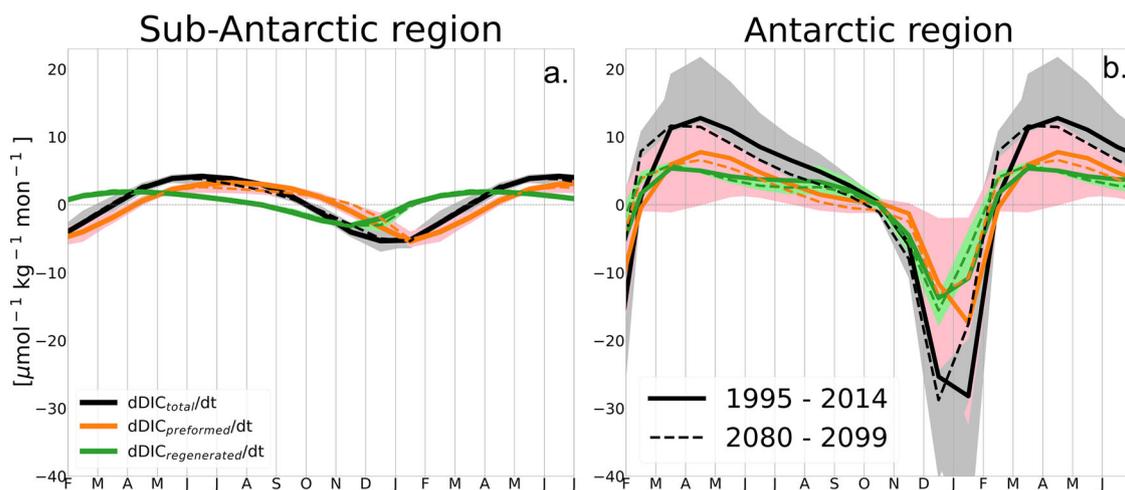
Fig. 6 | The decomposition of surface dissolved inorganic carbon (DIC) in the surface ocean. Current and projected rates of change of preformed (orange line), regenerated (green line) and total DIC (dDIC/dt, black) for the ensemble mean of IPSL-CM6A-LR, NorESM2-LM, and CMCC-ESM2 in **a** the Sub-Antarctic region and **b** Antarctic region. The shading in all figures shows the inter-model one standard deviation.

Fig. 2b). The Subtropics, therefore, has the highest seasonal warming and cooling rates in the contemporary Southern Ocean (Supplementary Fig. 3) and thus larger $(dpCO_2/dt)_T$ magnitudes in comparison to $(dpCO_2/dt)_{nonT}$ (Fig. 4d). This thermally dominated seasonal cycle in the Subtropics is well captured by ESMs; they show a relatively small model spread and compares well with the observed estimates (Fig. 4a). In the Sub-Antarctic region, the seasonal scale contribution of thermal and nonthermal processes have a near equal contribution ($M_{T-nonT} \sim 0$ atm mon^{-1}) and hence the seasonal cycle of ΔpCO_2 is generally less defined in comparison to the Subtropical and Antarctic regions (Fig. 4b, e & k). A full description of the thermal and nonthermal processes for the contemporary Sub-Antarctic region is provided in Supplementary Note 1.

In the Antarctic region, the seasonal cycle of pCO_2 is primarily non-thermally controlled for both pCO_2-products and ESMs in the contemporary climate (Fig. 4 l), ESMs show a large spread for both ΔpCO_2 and M_{T-nonT} in this region. The nonthermal processes that can be isolated from model outputs are net primary production, respiration and remineralization, indicators of mixing and stratification, and changes in sea-ice cover. We will use the apparent oxygen utilization (AOU) to estimate respiration, and will decompose the total rate of change of DIC into preformed and regenerated components (Figs. 5 and 6). AOU is defined as the difference between oxygen at saturation and the in situ dissolved oxygen concentration and it is used here to estimate respiration within the MLD[34]. Physical mixing processes will be here diagnosed through the rate of change of SST, mixed layer depth (MLD) and a stratification index based on the vertical density gradient (Figs. 5, 7). In addition, sea-ice is an essential distinguishing feature of Antarctic FCO_2 properties in comparison to the Sub-Antarctic and Subtropics. The seasonal presence of sea ice limits surface heat fluxes[35,36] constraining the SST to near freezing (Supplementary Fig. 1). This keeps the Antarctic SST rate of change relatively low (Fig. 5j & Supplementary Fig. 1), and hence the observed thermal pCO_2 component is lower than in the Subtropics and Sub-Antarctic region (Fig. 4f). While some ESMs shows this feature (e.g. CanESM5 and UKESM1-0LL, Supplementary fig. 3.), not all are consistent with the observed estimate, other models show a larger than observed rate of change of SST (Fig. 5j). ESMs also show a large model spread in the MLD (Fig. 5c, d) and stratification (Fig. 7a, b), which is overestimated in the Antarctic region. Model temperature bias in the Southern Ocean is a well-known feature of CMIP models since inception[37]. Some studies have linked this temperature bias to discrepancies in the simulated Atlantic Meridional Overturning Circulation (AMOC)[38,39], and other studies suggest that cloud-related biases overestimate the incoming shortwave flux[40,41]. These compounded effects influence the vertical heat

exchanges and stratification in the Antarctic region, and result in substantial model biases in the seasonal warming and cooling rates.

The seasonal presence of sea-ice also regulates biological and physical-driven variations of upper ocean DIC. The NPP seasonal cycle timing is linked to sea-ice variation in the Antarctic[36]; NPP increase initializes only after the sea-ice maximum (September), this leads to one to two months offset in comparison to the ice-free Sub-Antarctic (Fig. 5b, d). The NPP-related surface DIC consumption is evident in the negative DIC rate of change (Fig. 5f) during the high production season, and it coincides with the $(dpCO_2/dt)_{nonT}$ minima (Fig. 4f). Further, the timing of the NPP seasonal maxima also aligns with a minimum in the apparent oxygen utilization rate (Fig. 5h). Negative AOU rate of change reflects oxygen production during photosynthesis, whereas positive AOU rates of change is indicative of respiration or the oxidation of organic matter back to DIC in the near surface. Indeed, ESMs show positive AOU rate of change after the NPP maxima indicating subsequent remineralization. The alignment of AOU and DIC rates of change highlights that the role of biology in setting the DIC levels (Fig. 5a, b & e–h). Further, the decomposition of DIC into preformed and regeneration components (see methods for description, Eqs. 5–10) further substantiate that AOU is indeed a reliable indicator of biological-driven DIC variations (Fig. 6). Namely, $dDIC_{regenerated}/dt$, and $dAOU/dt$ display a similar seasonal cycle phasing, and both follows the NPP seasonality.

In addition to the NPP links to biological DIC variation in the upper ocean, NPP plays an essential role in regulating the physical DIC component[42,43]. According to the models, NPP levels sets vertical DIC gradients between the epipelagic and mesopelagic layers, which in turn determines the DIC entrainment rates during seasons (or events) of upper ocean mixing (Fig. 7). ESMs with high NPP tend to have stronger vertical DIC gradients (Fig. 7e, f, Supplementary Figs. 4d, f & 5a, b). The relationship between $(dDIC/dz)_{max}$ and seasonal NPP_{max} is robust in the Sub-Antarctic ($p < 0.01$) but is non-significant in the Antarctic region (Fig. 7e, f). We note that the low number of models may affect the significance in this region where models have a large spread in the seasonal sea-ice.

In summary, the processes characterizing the present-climate Southern Ocean DIC seasonality is primary production, respiration and entrainment mixing. In the Sub-Antarctic, entrainment fluxes are responsible for the DIC seasonal maximum; the dDIC/dt seasonal maximum occurs in early winter consistent with deep MLDs when maximum entrainment mixing is expected[44] (Fig. 5a). On the other hand, the dDIC/dt maximum occurs earlier than MLD maximum in the Antarctic, while MLDs are relatively shallow (~ 80 m) (Fig. 5b, f, h). In this region, the dDIC/dt maximum

Fig. 7 | Upper ocean dissolved inorganic carbon and density vertical gradients. a, b Vertical density gradient ($d\rho/dz$, top) and **c, d** vertical dissolved inorganic carbon gradient ($dDIC/dz$, middle panel) for the Sub-Antarctic (left) and Antarctic (right) regions. Blue lines depict the present climate (1995–2014), orange lines at the end of the 21st century (2080–2099), and black lines are observations (GLODAP) version 2 (2019). **e, f** Regression plots between the maximum annual primary production rate and the maximum subsurface DIC gradient for the contemporary climate (1995−2014). The shading in all figures shows the ensemble one standard deviation.
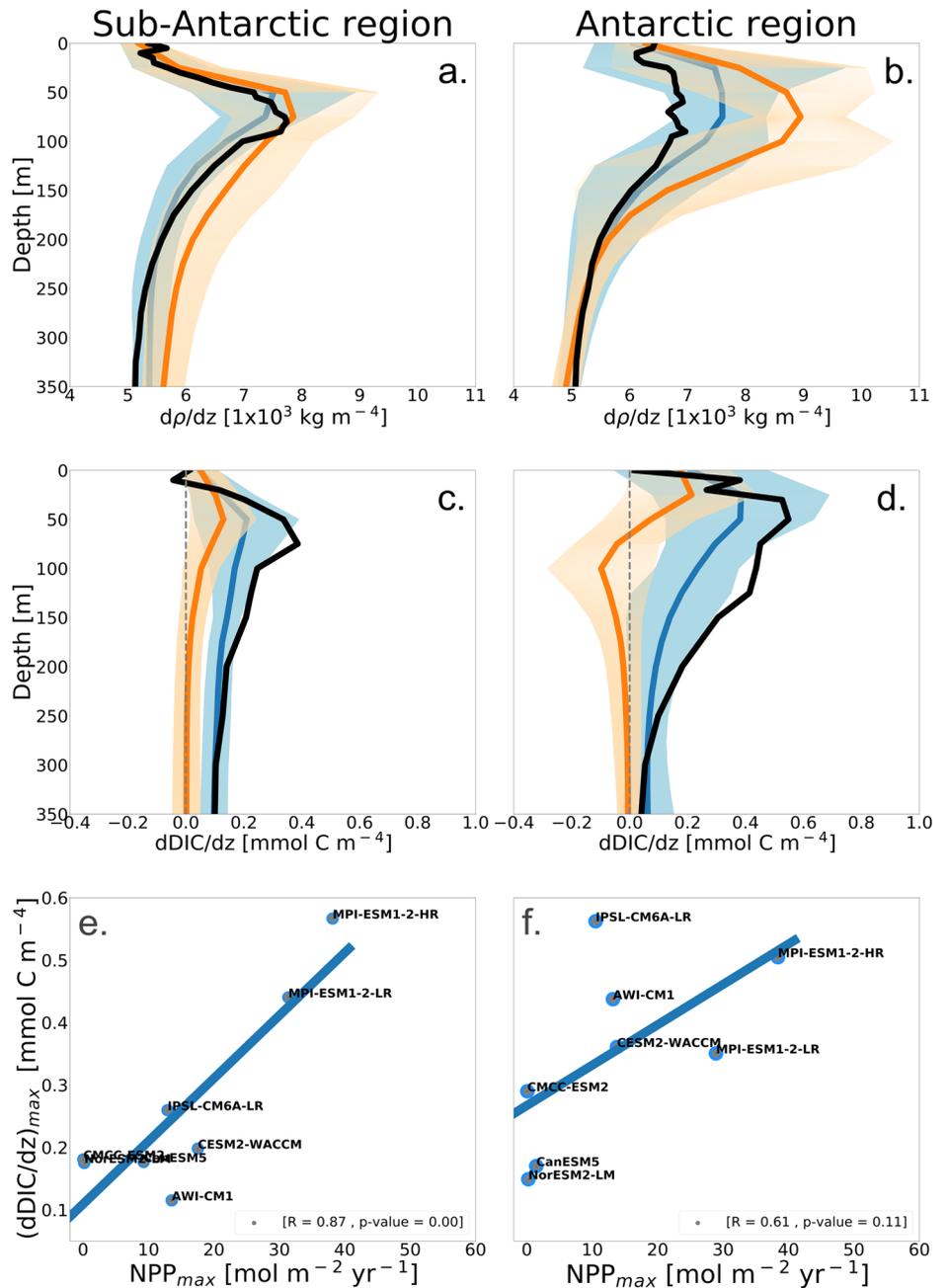
coincides with respiration and remineralization, as demonstrated by AOU and regenerated DIC (Figs. 5f, h and 6). The Antarctic DIC seasonal maximum is therefore first-order driven by near-surface respiration which peaks in autumn, but is sustained by entrainment mixing through winter when vertical mixing onsets in the models. This outcome suggests that the near surface respiration may be playing a more essential role than previously thought in the seasonal variations of surface DIC in the Antarctic region.

Poleward migration of the dominant CO₂ uptake zone in a warmer climate

At the end of the high emission scenario (2080–2099), the ocean is warmer; the Southern Ocean warms the most in the Subtropics (>3 °C), and the warming signal decreases poleward, reaching a maximum of 1 °C in the Antarctic by the end of the 21st century (Fig. 8d). Upwelling of the cool deep circumpolar water and sea-ice minimizes warming in the Antarctic region, keeping the surface waters relatively cool[40]. In the projected future, the surface ocean will be saltier in the Subtropics and fresher in the Antarctic region relative to the present climate (Supplementary Fig. 5e, f). Further, the increase of atmospheric CO_2 lowers the ocean CO_2 buffering capacity as the ocean take more CO_2, diagnosed by the increased Revelle Factor[11–13,17]. The combination of these factors leads to a poleward migration of the dominant region of CO_2 sink from the Subtropics to the Antarctic region (Fig. 8a, b). The mechanistic insight related to this poleward shift and why CO_2 uptake in the Subtropical region, although being the largest sink region in the present climate, do not increase as atmospheric CO_2 increase in the projected future is described below.

At the end of the 21st century, ΔpCO_2 annual averages change by nearly -150 µatm in the Antarctic region (>100 µatm model spread) and less than 50 µatm north of the Polar Front (Fig. 3f). North of the Polar Front, ΔpCO_2 seasonal averages (winter-summer) change has opposite signs and hence the annual mean is relatively small, whereas south of the Polar Front, ΔpCO_2 winter-summer averages have the same sign (Figs. 3 and 8c).
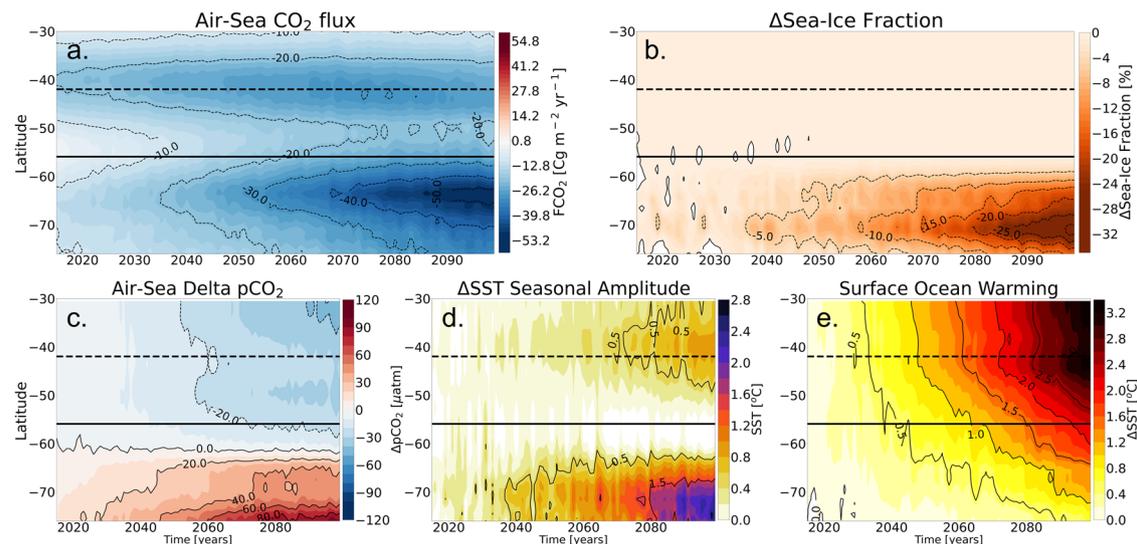
Fig. 8 | Summary figure for the drivers of the projected poleward shift in the dominant CO$_2$ sink region under high emissions. Annual and zonal mean air-sea CO$_2$ fluxes for the ensemble mean (FCO$_2$) south of 30 °S **a**, change in annual mean sea-ice fraction **b**, Air-sea ΔpCO$_2$ **c**, sea surface temperature seasonal amplitude **d** and surface ocean temperature with respect to the historical period (1995–2014) **e**.

Differences in the net ΔpCO$_2$ change north and south of the Polar Front at the end of century can be explained by differences in the relative contribution of the thermal and nonthermal pCO$_2$ components. In the Subtropics, the projected thermal component remains larger than the nonthermal contribution as in the present climate, and hence surface temperature remains the primary driver (Fig. 4 g, j). Therefore, higher atmospheric CO$_2$ enhances CO$_2$ uptake during cooler seasons when CO$_2$ solubility is high (autumn-winter) (Fig. 3e), but warming weakens CO$_2$ solubility in summer. This creates a positive feedback on the Subtropics CO$_2$ sink; the increase in CO$_2$ uptake during winter as atmospheric CO$_2$ increase is nearly all compensated by the weakening of CO$_2$ solubility in summer (Fig. 3d, e), and thus the net annual mean ΔpCO$_2$ is almost unchanged in the projected climate (Fig. 3f). The reduction of gas solubility in summer decreases the ΔpCO$_2$ which weakens CO$_2$ ingassing in the projected climate (Fig. 8c). The extension of the high emission scenario up to 2300 available for CanESM5 shows that the Subtropical CO$_2$ sink weakens post-2100 even though atmospheric CO$_2$ continues to rise (Supplementary Fig. 6), suggesting that the warming-driven weakening of CO$_2$ solubility becomes increasingly important as the ocean warms in the Southern Ocean except for the Antarctic region. ESMs general show a good agreement in simulating this mechanism in the Subtropics (Figs. 3–4), suggesting it is a robust feature under the high emission scenario.

In the Sub-Antarctic region, the sign of the projected M$_{T-nonT}$ (Fig. 4k) also remains unchanged with respect to the present climate; the majority of the ESMs still show a weak thermally driven seasonal cycle of ocean pCO$_2$ as in the present climate. The thermal and nonthermal components are increased by nearly equivalent amounts (Fig. 4h). Since the seasonal warming and cooling rates show little to no change in the projected climate (Fig. 5i), the increase in the thermal pCO$_2$ component is primarily due to the ocean pCO$_2$ increase (Eq. 1 in Methods). pCO$_2$ is more sensitivity to temperature in a high pCO$_2$ environment because of the Revelle factor increase[12]. The Revelle Factor increase enhances the sensitivity of pCO$_2$ to DIC and temperature changes, this effect increases poleward and is strongest in the Antarctic consistent with Revelle factor pattens[12,13,17] (Supplementary Fig. 11). In particular, the Revelle Factor increase enhances the sensitivity of pCO$_2$ to primary production and respiration (and mixing) driven DIC changes on the nonthermal pCO$_2$ components with nearly equivalent magnitudes but opposing directions (Fig. 4h, i). Although DIC rate of change declines in the projected future (Fig. 5e, f), its impact on the nonthermal pCO$_2$ contribution is larger than the present climate. This decline in DIC rates is driven by two factors. First, the upper ocean is more

stratified; stronger density vertical gradients (Fig. 7a, b) due to warming (Fig. 8e) and freshening of the upper ocean (Supplementary Fig. 5f, Fig. 5c, d). Secondly, the anthropogenic ocean DIC increase from rising atmospheric CO$_2$ propagates from the surface: DIC increases more at the surface than at depth (Supplementary Fig. 4), consequent weakening of the vertical DIC gradients (Fig. 7c, d), leading to a weaker DIC entrainment potential during vertical mixing. In summary, the impact of the Revelle factor increase partly self-compensates in Sub-Antarctic; it enhances the impact of mixing and respiration-driven DIC changes on surface pCO$_2$ in one direction, and primary production in the opposing direction, Fig. 4i.

In the Antarctic region, the magnitudes of the thermal and nonthermal components are also larger at the end of the 21st century compared to the present climate consistent with the expected Revelle factor increase in a high pCO$_2$ environment (Fig. 4i). Nevertheless, the warming-driven melting of sea-ice adds unique characteristics to how the Antarctic ocean pCO$_2$ and FCO$_2$ are impacted by the high atmospheric CO$_2$ and warming. We illustrate this by examining long-term changes on the thermal and nonthermal components. In addition to a lower CO$_2$ buffer capacity, dpCO$_{2T}$/dt magnitudes in the Antarctic increases by a larger margin in comparison to the ice-free regions because of the enhancements of seasonal cooling and warming rates related to sea-ice melt (Fig. 5j). The lengthening of open water seasons, and shallower MLDs due to warming and sea-ice melt (Fig. 5d) increases the summer-winter surface temperature contrast (Fig. 8d), leading to increases in the SST rate of change. The Antarctic surface waters require less energy to warm in the projected climate because of less sea-ice and shallower MLDs, this amplifies the seasonal warming and cooling rates, ultimately summer temperatures are higher than the present climate (Supplementary Fig. 1a, Fig. 8d). On the other hand, winter temperatures remain similar to the present climate because seasonal sea-ice growth is still present at the end of the century (Supplementary fig. 1a). Nevertheless, since not all Antarctic sea-ice is lost by the end of the century, surface waters remain cool even in late summer (below 5°C), and hence ocean CO$_2$ solubility increases (Supplementary Fig. 1a); this explains the ΔpCO$_2$ increase in the Antarctic (Fig. 8c). In summary, the Revelle factor increase, larger seasonal warming and cooling rates (Fig. 5j) together with higher ocean pCO$_2$ in the Antarctic leads to a larger thermal pCO$_2$ rates increase in comparison to the ice-free regions of the Southern Ocean (Fig. 4h, i).

Ultimately, the melting of sea-ice, stratification increase, MLD shallowing, DIC rates decline, and SST rates increase leads to a regime change in the primary driver of ocean pCO$_2$ from the nonthermal to thermal drivers in the winter to mid-spring seasons (JJASO) in the Antarctic region (Fig. 4l).

Article

Ocean pCO_2 shifts from the seasonal mixing-driven CO_2 outgassing in the present climate (Fig. 4l) to a solubility-driven CO_2 uptake during winter in the projected climate. The shift to gas solubility as the primary driver of ocean pCO_2 changes in winter allows ESMs to take up CO_2 in both the winter and summer seasons by a combination of solubility and biological CO_2 uptake. A higher Revelle factor also enhances the effect of biological driven DIC changes and hence CO_2 uptake in summer. Thus, ΔpCO_2 magnitudes in the Antarctic region have the same sign in winter and summer in the Antarctic, this leads to an extensive net annual mean ΔpCO_2 change in comparison to the Sub-Antarctic and Subtropical regions where ΔpCO_2 seasonal averages have opposing signs (Figs. 3 and 8c). The same-sign change in seasonal of ΔpCO_2 averages (Fig. 3d, f) in the Antarctic region also applies to ESMs with a year-round thermally-driven ocean pCO_2 (e.g. CanESM5 and NorESM2, Supplementary Fig. 10). Antarctic surface waters are constrained by seasonal sea-ice presence and upwelling of the circumpolar deep water from warming significantly above the freezing temperature (Fig. 8e). In contrast, sea-ice-free regions (Sub-Antarctic and Subtropical) are already significantly above freezing temperature (8 °C minimum, Supplementary Fig. 1), and hence further warming reduces gas solubility. In the Antarctic region, warming-driven sea-ice melt increase the volume of near freezing surface waters which has a lower molecular kinetic energy of CO_2 and therefore strengthening the solubility of atmospheric CO_2. Subsequently, warming reduces the ΔpCO_2 in the Subtropics and enhances it in the Antarctic (Fig. 8c). Thus, in principle, the Antarctic surface oceans can still take up CO_2 through gas solubility even at the end of the 21st century in the high-emission scenario. Therefore, in the projected climate, the Antarctic operates in a hybrid mode between biologically-driven summertime and solubility-driven wintertime uptake. While the analyzed ESMs show a large model spread in the Antarctic, the emergence of the Antarctic region as dominant CO_2 sink region in the projected climate is evident in all analyzed ESMs. This outcome suggests that although ESMs still show large differences the representation of biological and physical characteristics in the Antarctic region, the high-emission forcing projects a > 450% enhancement of the Antarctic CO_2 sink, suggesting this feature a robust.

Discussion

Examining multi-ESM projections of physical and biogeochemical processes, a robust pattern emerged whereby anthropogenic impacts manifested themselves through altering the seasonal carbon cycle with a large-scale shift in the CO_2 uptake region from the Subtropics to the Antarctic region. This major finding was robust even when accounting for uncertainties in multi-model projections.

Mechanistically, it is caused by a change in the mechanisms of seasonal CO_2 uptake in the Antarctic (Figs. 1–2, 8a) causing a poleward migration of the dominant CO_2 uptake region. This poleward shift in the region of the largest CO_2 sink was noticed by earlier studies[16,45,46] without mechanistic links to seasonal carbon dynamics at polar latitudes. A recent study[26] based on a single ESM showed that warming enhances the outgassing of natural CO_2 under the high-emission scenario, which explains the decline of subtropical uptake. The Antarctic is a challenging region to model ocean carbon cycling. ESMs show a large spread and extensive biases with respect to observations for ΔpCO_2, MLD, DIC, and thermal & nonthermal pCO_2 components (Figs. 4–5). Relatively low model skill in the Antarctic region is partly due to known biases in sea ice[35,47–49], cloud-related shortwave biases impact on heat fluxes[38,40], the AMOC[37,50] and their related stratification biases, which reflect on the simulated biological properties, e.g., phytoplankton phenology[36]. This is because sea-ice extent and seasonality are central in setting the timing of the biologically-driven DIC variability, and the respiration-entrainment mixing driven CO_2 outgassing in the contemporary Antarctic region; seasonal FCO_2 variability, and uptake (Figs. 5–8). With these uncertainties in mind, this multi-model study provides two further insights in the poleward migration of the largest CO_2 sink in the Southern Ocean under the high-emission scenario.

First, the melting of sea-ice plays a major role in setting the conditions for the major shift in the Antarctic region. The melting of sea-ice will freshen and stratify the upper ocean, which on the one hand shoals and decreases the differences in MLD seasonal characteristics among ESMs, reducing the model spread significantly by the end of the 21st century (Fig. 5d). It remains unclear why ESM's MLD differences are reduced under the high-emission scenario. The role of sea-ice melt is well illustrated by a stronger corelation between sea-ice loss and FCO_2 post-2060 (Fig. 8a, b) when sea-ice loss surpasses 5-10%. It is at this stage (post-2060) that the domain of the largest CO_2 uptake transitions to the Antarctic region (Fig. 8a). The strong correlation between CO_2 uptake and sea-ice melt post-2060 reinforces the central role of sea-ice in driving the CO_2 dynamics of the Antarctic, and further highlights the importance of improving the representation of sea-ice in ESMs among other biases (Fig. 8a, b). Moreover, links between sea-ice changes and CO_2 uptake through solubility elevate the role of solubility as an important mechanism of CO_2 uptake in the Southern Ocean. The largest CO_2 sink domain in the present climate and projected climate resides where solubility plays a primary role. Surface warming weakens the solubility in CO_2 uptake in the Subtropics and enhances through sea-ice melt in the Antarctic. Beyond 2100, the high warming scenario in CanESM5 shows that the Subtropics cease to take up CO_2 although atmospheric CO_2 is still growing while the Antarctic region becomes even a stronger sink of CO_2 (Supplementary Fig. 6). This suggests that climate change will have regionally variable effect on the Southern Ocean FCO_2. Understanding the mechanisms behind this regional difference will be crucial to improve model projections, and elucidate the broader climate and ecosystems impacts.

Secondly, the accumulation of anthropogenic carbon in the upper ocean in the high warming scenario diminishes (or even reverses) the vertical gradient of DIC (Figs. 6–7). This mechanism works through the shift in the seasonal cycle of upper ocean DIC balance. The wintertime entrainment of DIC is reduced due to the weakened vertical gradients of DIC, leading to the dominance of thermally-driven pCO_2 changes (Figs. 4l and 7). This sets up the seasonal regime change to the thermally-driven CO_2 uptake in the Antarctic region.

This outcome suggest that solubility-induced carbon uptake may be as important or even possibly more important than biological CO_2 uptake during major climate transitions[51,52]. Although biological CO_2 uptake is an essential mechanism for CO_2 uptake in the Southern Ocean[34,46,53] and has been shown to play a key role in glacial time scale regime changes[54,55]. Biological CO_2 uptake alone is partly offset by the remineralization of organic matter post-production, limiting its role in CO_2 uptake in the Southern Ocean. Because of this respiration effect[56], even if primary production were to increase in the projected climate, respiration will likely partly compensate for the CO_2 uptake due to a larger Revelle factor. On the other hand, CO_2 solubility is capable of becoming an important contributor to CO_2 uptake when sea-ice melt is evident by subverting the role of near-surface respiration and/or seasonal mixing in winter CO_2 outgassing through the shifting surface carbonate system to a thermally driven system. We postulate that this solubility feature is only active during relatively cool sea surface temperatures to allow solubility-driven CO_2 ingassing. If the polar oceans were to warm significantly above the freezing temperature, the drivers of FCO_2 may become similar to the Subtropical region or the Arctic Ocean, where warming reduces kinematic gas solubility[57]. Further warming and complete loss of sea ice in the Arctic for example has been shown to cause the reversal of the seasonal cycle of ocean pCO_2 under the high-emission scenario in the projected climate[57]. This type of regime change is however unlikely to occur in the Southern Ocean because of dynamic differences. The Arctic Ocean relies on winter mixing to entrain nutrients and export carbon to the deep ocean and is thus more affected by global warming through stratification[52]. In contrast, westerly winds in the Southern Ocean will likely continue to provide the main forcing for the upwelling of cold and nutrient-rich water[58]. Instead, we postulate that the future of the polar Southern Ocean may operate in a hybrid mode of biologically-driven summertime uptake and solubility-driven wintertime uptake, taking a leading role in the projected Southern Ocean carbon sinks.

Sustaining carbon uptake in the polar Southern Ocean requires a mechanism to export the excess carbon into the interior ocean, away from the region of uptake. A recent study[45] demonstrated that the increased CO_2 sink south of the Polar Front under the high-emission scenario was linked to the Southern Ocean's ability to advect subsurface low DIC waters equatorward allowing a continuous surface uptake of atmospheric CO_2. The long-term perspective of this carbon sink may depend on the circulation changes that transfer carbon absorbed from the atmosphere to the water masses in the intermediate and deep-water reservoirs. On the other hand, anthropogenic ice sheet melt in Antarctica is projected to slow down the Southern Ocean overturning and enhance surface stratification[41] which may weaken this northward DIC advection. Moreover, ice sheet melt is also projected to enhance Antarctic sea-ice and slow-down warming through the albedo feedback[38,41]. Stronger stratification may continue to constrain winter DIC surface-subsurface mixing and allowing the surface ocean to take up CO_2 through solubility in winter although sea-ice is abundant, but this CO_2 sink may eventually be weakened by poor overturning. It remains unclear how these processes will work together; the inclusion interactive ice sheet in the next generation of ESMs will be key to understanding this mechanism.

Methods

Earth system models
We use the output from nine CMIP6 ESMs (Supplementary Table 1), contrasting the contemporary period (1995–2014) and the end of the 21st century (2080–2099) under the socioeconomic pathway 5–8.5 (SSP5–8.5) climate scenario[59]. Model selection was based on the availability of essential variables at the time of writing; we used a single ensemble member for each model. All ESMs output was downloaded from the earth system grid federation (ESGF) hosted at the German climate computing center (DKRZ, https://esgf-node.llnl.gov/search/cmip6/) except for AWI-CM1. The downloaded model output was stored and analyzed on the Cheyenne National Center for Atmospheric Science (NCAR) server. The following fields were downloaded: monthly mean surface ocean partial pressure of carbon dioxide (spco2), air-sea delta pCO2 (dpco2), air-sea CO_2 flux (fgco2), total dissolved inorganic carbon (dissic), total ocean alkalinity (talk), sea surface temperature (tos), sea surface salinity (sos), net primary production (intpp), mixed layer depth (mlotst), sea ice fraction (siconc), dissolved oxygen (o2), dissolved oxygen at saturation (o2sat), practical ocean salinity (so) and potential temperature (thetao). Since not all ESMs have the complete output variables available at the time of writing, some figures do not display all ESMs. Model outputs were analyzed on their native grids except for the unstructured mesh ocean model of AWI-CM1, which was regridded to a 1° × 1° regular grid. Stereographic projection figures (Fig. 1 was made using 1° × 1° regular grid data.

Observation-based pCO₂-products
We use six observation-based surface pCO2 products available in the Sea-Flux dataset[60] downloaded from: https://zenodo.org/record/5482547. The individual products are: CMEMS-LSCE-FFNN[61]; CSIR-ML6[62]; Jena-MLS[63]; JMA-MLR[64]; MPI-SOMFFN[59]; and NIES-FNN[65]—see Supplementary Fig. Table 2 for more details. The pCO2 products fill the gaps in sparse ship-based observations of pCO2 with satellite observations, reanalyzes outputs, and observational monthly climatologies. Statistical models (e.g., artificial neural networks) are used to estimate the relationship between proxy variables and pCO2, meaning that these approaches incorporate little to no mechanistic understanding of the drivers of pCO2. Proxy variables include, but are not limited to: sea surface temperature (remote sensing), salinity (reanalysis), mixed layer depth (climatology), and ocean color estimates of phytoplankton chlorophyll which is understood as a proxy for biomass (remote sensing). All methods use pCO2 from the Surface Ocean CO_2 Atlas (SOCAT version 2020 or later)[66]. All observation-based products are estimated on or re-gridded to a monthly 1° × 1° regular grid. Further, we use the ocean potential temperature and salinity dataset from the World Ocean Atlas[67] to estimate observed vertical density. We use a monthly climatology of mixed layer depth by[68,69] based on various temperature and salinity

profiling instruments to compare with model output. Lastly, we use DIC from the Global Ocean Data Analysis Project (GLODAP) version 2 (2019) dissolved inorganic carbon dataset[41] to compare with models.

Thermal and nonthermal ocean pCO₂ decomposition
Surface ocean pCO2 and ΔpCO2 variability is controlled by the relative contribution of thermal and nonthermal components[28,29]. We here estimate the thermal component using the Takahashi et al.[30] formulation[30] (Eqs. 1–2) and we estimate the nonthermal component by subtracting the thermal component from the total (Eq. 3). Thermal component is driven by temperature variations through changes in gas solubility (Henry's law). The nonthermal pCO2 component on other hand is mainly controlled by mixing and biology[31], which also includes the role of total alkalinity and salinity changes. However, total alkalinity and salinity have been shown to play a minor role in the seasonal cycle of ocean pCO2 in the contemporary Southern Ocean[29,31], thus, here we focus on processes responsible for sources and sinks of DIC, i.e., primary production, respiration, and seasonal buoyancy change-driven mixing. The thermal and nonthermal components of pCO2 oppose each other on a seasonal scale[32,33] (Fig. 4d, f), and hence the larger of the two determines the observed seasonal cycle phasing of pCO2, and ultimately FCO2[29]. The relative contributions of thermal and nonthermal components are assessed here through the absolute difference in their monthly rates (M_{T-nonT}, Eq. 4). The larger rate of change between $|(dpCO_2/dt)_T|$ and $|(dpCO_2/dt)_{nonT}|$ is therefore considered the dominant driver of ocean surface pCO2 change (monthly in our case). This is estimated by the absolute difference of the time derivative of the thermal and nonthermal components, and we term this diagnostic metric as M_{T-nonT} (Eq. 3), consistent with Mongwe et al.[29]. $M_{T-nonT} > 0$ indicates periods when temperature variance drives the pCO2, while $M_{T-nonT} < 0$ is indicative of periods when nonthermal processes play a leading role in surface pCO2. While simple, M_{T-nonT} provides a useful diagnostic for identifying the predominant mechanisms driving seasonal pCO2 variations, in particular, given that the thermal and nonthermal pCO2 oppose each other on a seasonal scale, thus isolating the leading driver provides key information.

$$pCO_{2T} = 0.0423 \times \overline{pCO_2} \times SST \qquad (1)$$

$$\left(\frac{\partial pCO_2}{\partial t}\right)_T = 0.0423 \times \overline{pCO_2} \times \left(\frac{\partial SST}{\partial t}\right) \qquad (2)$$

$$\left(\frac{\partial pCO_2}{\partial t}\right)_{nonT} = \left(\frac{\partial pCO_2}{\partial t}\right)_{Tot} - \left(\frac{\partial pCO_2}{\partial t}\right)_T \qquad (3)$$

$$M_{T-nonT} = \left|\left(\frac{\partial pCO_2}{\partial t}\right)_T\right| - \left|\left(\frac{\partial pCO_2}{\partial t}\right)_{nonT}\right| \qquad (4)$$

DIC decomposition
The variability of ocean DIC outside of external drives is driven by ocean physical (circulation and mixing) and biological processes (i.e. primary production and respiration)[70,71]. DIC is consumed through photosynthesis to form organic matter in the upper ocean and is produced by the reverse process of respiration in the near surface to the deep ocean, where organic matter is remineralized, this component of DIC is referred to as regenerated DIC[70,72]. The non-biological component of DIC is mainly controlled by the subduction at mass transformation and mixing is referred to as preformed DIC. In this study, we decompose the surface DIC seasonal cycle into preformed and regenerated following[70,72] (Eq. 5). Regenerated DIC comprises of the soft pump, which represents the biological production and remineralization of particulate organic carbon (C^{soft}, Eq. 7), and the carbonate part representing the consumption and remineralisation of molecularly charged nutrients (Eq. 8)[72]. Since our analysis is focused on the surface ocean, we assume that Talk = Talk^{pre}, hence Eq. 8 excludes the total alkalinity contribution. Preformed DIC comprises of the saturated DIC

concentration in equilibrium with the atmosphere (C^{sat}), and the disequilibrium contribution; estimates deviations from C^{ast} when mixing occurs before air-sea exchange is complete (C^{dis})[70,73–75]. $R_{C:O_2}$ is the carbon to oxygen stoichiometric ratio (-106/170), $R_{N:O_2}$ is the stoichiometric ratio of nitrate to oxygen (-16/170), S is salinity, T is surface temperature, O_2^{sat} is oxygen at saturation, O_2 is dissolved oxygen and AOU is the apparent utilization of oxygen.

$$DIC = C^{pre} + C^{reg} \tag{5}$$

$$C^{reg} = C^{soft} + C^{carb} \tag{6}$$

$$C^{soft} = -R_{C:O_2} \times AOU \tag{7}$$

$$C^{carb} = \frac{1}{2}\left(-R_{N:O_2} \times AOU\right) \tag{8}$$

$$AOU = O_2^{sat}(T, S) - O_2) \tag{9}$$

$$C^{pre} = C^{sat} + C^{dis} \tag{10}$$

Study domain

In this study, we divide the Southern Ocean into three subdomains using dynamical frontal boundaries to reflect the three regimes of the Southern Ocean. Namely, (i) the Subtropical region, the warmest and most stratified part of the Southern Ocean, (ii) the Sub-Antarctic region, highly productive, moderately warm, and host the subduction of the Subantarctic Mode Water and Antarctic Intermediate Waters; and (iii) the Antarctic region, seasonally productive, cool, seasonally sea-ice covered and upwelling region. We use the[76] dynamical boundary definition based on potential temperature, (i) the Subtropical region is between 30 °S and the Subtropical Front, (ii) the Sub-Antarctic region between the Subtropical Front and Polar Front; and (iii) the Antarctic region, south of the Polar Front to the sea-ice edge or continental margin. Orsi et al.[76] boundaries are nearly similar to the commonly used typical Fay and McKinley et al.[50] biomes but differ most in the Subtropical region, where the Fay and McKinley biomes exclude a large part of the subtropical Pacific. Furthermore, not all the analyzed ESMs have all the required output to estimate the[50] biomes for both the present climate and the end of the century. Dynamic boundaries are calculated for each model and averaged for the present climate (1995–2014) and end of the 21st century (2080–2099). And for the observed estimate we use the same dynamic boundary based on the WOA dataset. Regional averages are estimate using each model's native dynamic boundary and averaged for the ensemble mean afterward.

Data availability

The coupled model intercomparison project (CMIP) version 6 earth system model output used in this study is publicly at the German climate computing center (DKRZ, https://esgf-node.llnl.gov/search/cmip6/). The six observation-based surface pCO_2 products available in the SeaFlux dataset[60] (https://zenodo.org/record/5482547). Temperature and Salinity data we used the from the world ocean atlas version 2013 can be accessed in https://www.ncei.noaa.gov/data/oceans/woa/WOA13/DATAv2/. Dissolved inorganic carbon (DIC) Global Ocean Data Analysis Project (GLODAP) version 2 (2019) is publicly available at https://glodap.info/index.php/merged-and-adjusted-data-product-v2−2019/. The mixed layer data is available at https://cerweb.ifremer.fr/deboyer/mld/Surface_Mixed_Layer_Depth.php. The datasets behind Figs. 1–8 can be found in Supplementary Data 1.

Code availability

The scripts and source data used to produce figures in this paper are available in https://zenodo.org/records/10895388.

References

1. Frölicher, T. L. et al. Dominance of the Southern Ocean in anthropogenic carbon and heat uptake in CMIP5 models. *J. Clim.* **28**, 862–886 (2015).
2. Fung, I. Y., Doney, S. C., Lindsay, K. & John, J. Evolution of carbon sinks in a changing climate. *Proc. Natl. Acad. Sci. USA* **102**, 11201–11206 (2005).
3. Khatiwala, S., Primeau, F. & Hall, T. Reconstruction of the history of anthropogenic CO2 concentrations in the ocean. *Nature* **462**, 346–349 (2009).
4. Gruber, N. et al. The oceanic sink for anthropogenic CO_2 from 1994 to 2007. *Science* **363**, 1193–1199 (2019).
5. Palter, J. B., Sarmiento, J. L., Gnanadesikan, A., Simeon, J. & Slater, R. D. Fueling export production: Nutrient return pathways from the deep ocean and their dependence on the Meridional Overturning Circulation. *Biogeosciences* **7**, 3549–3568 (2010).
6. Holzer, M. & Primeau, F. W. Global teleconnections in the oceanic phosphorus cycle: Patterns, paths, and timescales. *J. Geophys. Res. Oceans* **118**, 1775–1796 (2013).
7. Primeau, F. W., Holzer, M. & DeVries, T. Southern Ocean nutrient trapping and the efficiency of the biological pump. *J. Geophys. Res. Oceans* **118**, 2547–2564 (2013).
8. Bourgeois, T., Goris, N., Schwinger, J. & Tjiputra, J. F. Stratification constrains future heat and carbon uptake in the Southern Ocean between 30°S and 55°S. *Nat. Commun.* **13**, 340 (2022).
9. Terhaar, J., Frölicher, T. L. & Joos, F. Southern Ocean anthropogenic carbon sink constrained by sea surface salinity. *Sci. Adv.* **7**, 5964–5992 (2021).
10. Bindoff, N. L. et al. Changing Ocean, Marine Ecosystems, and Dependent Communities. In *IPCC Special Report on the Ocean and Cryosphere in a Changing Climate* (eds. Pörtner H. -O. et al.) pp. 447–587 (Cambridge University Press, Cambridge, New York, USA, 2019).
11. Gidden, M. J. et al. Global emissions pathways under different socioeconomic scenarios for use in CMIP6: A dataset of harmonized emissions trajectories through the end of the century. *Geosci Model Dev.* **12**, 1443–1475 (2019).
12. Fassbender, A. J., Schlunegger, S., Rodgers, K. B. & Dunne, J. P. Quantifying the role of seasonality in the marine carbon cycle feedback: an ESM2M case study. *Glob. Biogeochem. Cycles* **36**, 1–15 (2022).
13. Fassbender, A. J., Sabine, C. L. & Palevsky, H. I. Nonuniform ocean acidification and attenuation of the ocean carbon sink. *Geophys. Res. Lett.* **44**, 8404–8413 (2017).
14. Moore, J. K. et al. Sustained climate warming drives declining marine biological productivity. *Science (1979)* **359**, 1139–1143 (2018).
15. Kwiatkowski, L. et al. Twenty-first century ocean warming, acidification, deoxygenation, and upper-ocean nutrient and primary production decline from CMIP6 model projections. *Biogeosciences* **17**, 3439–3470 (2020).
16. Chikamoto, M. O. & DiNezio, P. Multi-Century Changes in the Ocean Carbon Cycle Controlled by the Tropical Oceans and the Southern Ocean. *Global Biogeochem. Cycles* **35**, 1–16 (2021).
17. Hauck, J. & Völker, C. Rising atmospheric CO2 leads to large impact of biology on Southern Ocean CO2 uptake via changes of the Revelle factor. *Geophys. Res. Lett.* **42**, 1459–1464 (2015).
18. Kwiatkowski, L. & Orr, J. C. Diverging seasonal extremes for ocean acidification during the twenty-first century. *Nat. Clim. Chang.* **8**, 141–145 (2018).
19. Wanninkhof, R., Asher, W. E., Ho, D. T., Sweeney, C. & McGillis, W. R. Advances in quantifying air-sea gas exchange and environmental forcing. *Ann. Rev. Mar. Sci.* **1**, 213–244 (2009).

20. Lévy, M. et al. Contribution of tropical cyclones to the air-sea CO 2 flux: a global view. *Glob. Biogeochem. Cycles* **26**, 1–8 (2012).

21. Landschützer, P. et al. The reinvigoration of the Southern Ocean carbon sink. *Science* **349**, 1221–1224 (2015).

22. Monteiro, P. M. S. et al. Intraseasonal variability linked to sampling alias in air-sea CO2 fluxes in the Southern Ocean. *Geophys Res Lett* **42**, 8507–8514 (2015).

23. Bushinsky, S. M., Takeshita, Y. & Williams, N. L. Observing Changes in Ocean Carbonate Chemistry: Our Autonomous Future. *Curr. Clim. Change Rep.* **5**, 207–220 (2019).

24. Sutton, A. J., Williams, N. L. & Tilbrook, B. Constraining Southern Ocean CO_2 Flux Uncertainty Using Uncrewed Surface Vehicle Observations. *Geophys. Res. Lett.* **48**, e2020GL091748 (2021).

25. Nicholson, S. A. et al. Storms drive outgassing of CO_2 in the subpolar Southern Ocean. *Nat. Commun.* **13**, 158 (2022).

26. Lerner, P. et al. Drivers of air-Sea CO_2 flux seasonality and its long-term changes in the NASA-GISS Model CMIP6 submission. *J. Adv. Model Earth Syst.* **13**, 1–33 (2021).

27. Monteiro, T., Kerr, R. & Machado, E. D. C. Seasonal variability of net sea-air CO_2 fluxes in a coastal region of the northern Antarctic Peninsula. *Sci. Rep.* **10**, 14875 (2020).

28. Takahashi, T. et al. Global sea-air CO_2 flux based on climatological surface ocean pCO_2, and seasonal biological and temperature effects. *Deep Sea Research Part II: Topical Studies in Oceanography* **49**, 1601–1622 (2002).

29. Mongwe, N. P., Vichi, M. & Monteiro, P. M. S. The seasonal cycle of pCO2 and CO2 fluxes in the Southern Ocean: Diagnosing anomalies in CMIP5 Earth system models. *Biogeosciences* **15**, 2851–2872 (2018).

30. Takahashi, T., Olafsson, J., Goddard, J. G., Chipman, D. W. & Sutherland, S. C. Seasonal variation of CO_2 and nutrients in the high-latitude surface oceans: a comparative study. *Glob. Biogeochem. Cycles* **7**, 843–878 (1993).

31. Lauderdale, J. M., Dutkiewicz, S., Williams, R. G. & Follows, M. J. Quantifying the drivers of ocean-atmosphere CO2 fluxes. *Global Biogeochem Cycles* **30**, 983–999 (2016).

32. Gruber, N., Landschützer, P., Landschützer, L. & Lovenduski, N. S. The Variable Southern Ocean Carbon Sink. *Annu. Rev. Mar. Sci.* **11**, 159–186 (2019).

33. Angeles Gallego, M., Timmermann, A., Friedrich, T. & Zeebe, R. E. Drivers of future seasonal cycle changes in oceanic pCO2. *Biogeosciences* **15**, 5315–5327 (2018).

34. Sarmiento, J. L. & Gruber, N. *Ocean Biogeochemical Dynamics* (Princeton University Press, Princeton, 2006).

35. Shu, Q. et al. Assessment of Sea Ice Extent in CMIP6 With Comparison to Observations and CMIP5. *Geophys. Res. Lett.* **47**, e2020GL087965 (2020).

36. Hague, M. & Vichi, M. A Link Between CMIP5 Phytoplankton Phenology and Sea Ice in the Atlantic Southern Ocean. *Geophys. Res. Lett.* **45**, 6566–6575 (2018).

37. Farneti, R., Stiz, A. & Ssebandeke, J. B. Improvements and persistent biases in the southeast tropical Atlantic in CMIP models. *NPJ Clim. Atmos. Sci.* **5**, 42 (2022).

38. Wang, C., Zhang, L., Lee, S. K., Wu, L. & Mechoso, C. R. A global perspective on CMIP5 climate model biases. *Nat. Clim. Chang.* **4**, 201–205 (2014).

39. Luo, F., Ying, J., Liu, T. & Chen, D. Origins of Southern Ocean warm sea surface temperature bias in CMIP6 models. *NPJ Clim. Atmos. Sci.* **6**, 127 (2023).

40. Morrison, A. K., Waugh, D. W., Hogg, A. M., Jones, D. C. & Abernathey, R. P. Ventilation of the Southern Ocean Pycnocline. *Annual Review of Marine Science* **26**, 405–430 (2022).

41. Hyder, P. et al. Critical Southern Ocean climate model biases traced to atmospheric model cloud errors. *Nat. Commun.* **9**, 3625 (2018).

42. Moore, T. S. et al. Sea surface pCO_2 and O_2 in the Southern Ocean during the austral fall, 2008. *J. Geophys. Res. Oceans* **116**, C00F11 (2011).

43. Dufour, C. O. et al. Eddy compensation and controls of the enhanced sea-to-air CO2 flux during positive phases of the Southern Annular Mode. *Global Biogeochem. Cycles* **27**, 950–961 (2013).

44. Libera, S., Hobbs, W., Klocker, A., Meyer, A. & Matear, R. Ocean-sea ice processes and their role in multi-month predictability of antarctic sea ice. *Geophys. Res. Lett.* **49**, e2021GL097047 (2022).

45. Tjiputra, J. F., Assmann, K. & Heinze, C. Anthropogenic carbon dynamics in the changing ocean. *Ocean Sci.* **6**, 605–614 (2010).

46. Hauck, J. et al. On the Southern Ocean CO_2 uptake and the role of the biological carbon pump in the 21st century. *Global Biogeochem. Cycles* **29**, 1451–1470 (2015).

47. Turner, J., Bracegirdle, T. J., Phillips, T., Marshall, G. J. & Scott Hosking, J. An initial assessment of Antarctic sea ice extent in the CMIP5 models. *J. Clim.* **26**, 1473–1484 (2013).

48. Meijers, A. J. S. The Southern Ocean in the Coupled Model Intercomparison Project phase 5. *Philo. Trans. R. Soc. A: Math. Phys. Eng. Sci.* **372**, 20130296 (2014).

49. Roach, L. A. et al. Antarctic Sea Ice Area in CMIP6. *Geophys. Res. Lett.* **47**, e2019GL086729 (2020).

50. Fay, A. R. & McKinley, G. A. Global open-ocean biomes: Mean and temporal variability. *Earth Syst. Sci. Data* **6**, 273–284 (2014).

51. Dai, Y., Yu, J., Ren, H. & Ji, X. Deglacial Subantarctic CO_2 outgassing driven by a weakened solubility pump. *Nat. Commun.* **13**, 5193 (2022).

52. Farmer, J. R. et al. Arctic Ocean stratification set by sea level and freshwater inputs since the last ice age. *Nat. Geosci.* **14**, 684–689 (2021).

53. Marinov, I., Gnanadesikan, A., Toggweiler, J. R. & Sarmiento, J. L. The Southern Ocean biogeochemical divide. *Nature* **441**, 964–967 (2006).

54. Gottschalk, J. et al. Biological and physical controls in the Southern Ocean on past millennial-scale atmospheric CO_2 changes. *Nat. Commun.* **7**, 11539 (2016).

55. Khatiwala, S., Schmittner, A. & Muglia, J. Climatology Air-sea disequilibrium enhances ocean carbon storage during glacial periods. *Sci. Adv.* **5**, eaaw4981 (2019).

56. Chen, H., Haumann, F. A., Talley, L. D., Johnson, K. S. & Sarmiento, J. L. The Deep Ocean's Carbon Exhaust. *Global Biogeochem. Cycles* **36**, e2021GB007156 (2022).

57. Orr, J. C., Kwiatkowski, L. & Pörtner, H. O. Arctic Ocean annual high in pCO2 could shift from winter to summer. *Nature* **610**, 94–100 (2022).

58. Zickfeld, K., Fyfe, J. C., Saenko, O. A., Eby, M. & Weaver, A. J. Response of the global carbon cycle to human-induced changes in Southern Hemisphere winds. *Geophys. Res. Lett.* **34**, L12712 (2007).

59. Iida, Y., Takatani, Y., Kojima, A. & Ishii, M. Global trends of ocean CO2 sink and ocean acidification: an observation-based reconstruction of surface ocean inorganic carbon variables. *J. Oceanogr.* **77**, 323–358 (2021).

60. Eyring, V. et al. Overview of the Coupled Model Intercomparison Project Phase 6 (CMIP6) experimental design and organization. *Geosci. Model Dev.* **9**, 1937–1958 (2016).

61. Fay, A. R. et al. SeaFlux: Harmonization of air-sea CO_2 fluxes from surface pCO2 data products using a standardized approach. *Earth System Science Data* **13**, 4693–4710 (2021).

62. Denvil-Sommer, A., Gehlen, M. & Vrac, M. Observation system simulation experiments in the Atlantic Ocean for enhanced surface ocean pCO2 reconstructions. *Ocean Sci.* **17**, 1011–1030 (2021).

63. Gregor, L., Lebehot, A. D., Kok, S. & Scheel Monteiro, P. M. A comparative assessment of the uncertainties of global surface ocean CO2 estimates using a machine-learning ensemble (CSIR-ML6 version 2019a)-Have we hit the wall? *Geosci. Model Dev.* **12**, 5113–5136 (2019).

64. Rödenbeck, C. et al. Global surface-ocean pCO2 and sea-Air CO_2 flux variability from an observation-driven ocean mixed-layer scheme. *Ocean Sci.* **9**, 193–216 (2013).

65. Landschützer, P., Gruber, N., Bakker, D. C. E. & Schuster, U. Recent variability of the global ocean carbon sink. *Glob. Biogeochem. Cycles* **28**, 927–949 (2014).

66. Zeng, J., Nojiri, Y., Landschützer, P., Telszewski, M. & Nakaoka, S. A global surface ocean fCO_2 climatology based on a feed-forward neural network. *J. Atmos. Ocean Technol.* **31**, 1838–1849 (2014).

67. Bakker, D. C. E. et al. A multi-decade record of high-quality fCO_2 data in version 3 of the Surface Ocean CO_2 Atlas (SOCAT). *Earth System Science Data* **8**, 383–413 (2016).

68. Locarnini, R. A. et al. Word ocean atlas 2013. Volume 1: Temperature http://www.nodc.noaa.gov/ (2013).

69. de Boyer Montégut, C., Madec, G., Fischer, A. S., Lazar, A. & Iudicone, D. Mixed layer depth over the global ocean: An examination of profile data and a profile-based climatology. *J. Geophys. Res. Oceans* **109**, 1–20 (2004).

70. Sadai, S., Condron, A., DeConto, R. & Pollard, D. Future climate response to Antarctic Ice Sheet melt caused by anthropogenic warming. *Sci. Adv.* **6**, eaaz1169 (2020)

71. Golledge, N. R. et al. Global environmental consequences of twenty-first-century ice-sheet melt. *Nature* **566**, 65–72 (2019).

72. Ito, T. & Follows, M. J. Preformed phosphate, soft tissue pump and atmospheric CO_2. *Journal of Marine Research*. **63**, 813– 839 (2005).

73. Ito, T., Follows, M. J. & Boyle, E. A. Is AOU a good measure of respiration in the oceans? *Geophys. Res. Lett.* **31**, L17305 (2004).

74. Lauderdale, J. M., Garabato, A. C. N., Oliver, K. I. C., Follows, M. J. & Williams, R. G. Wind-driven changes in Southern Ocean residual circulation, ocean carbon reservoirs and atmospheric CO_2. *Clim. Dyn.* **41**, 2145–2164 (2013).

75. Ito, T., Marshall, J. & Follows, M. What controls the uptake of transient tracers in the Southern Ocean? *Glob. Biogeochem. Cycles* **18**, 1–17 (2004).

76. Orsi, A. H., Whitworth, T. & Nowlin, W. D. On the meridional extent and fronts of the Antarctic Circumpolar Current. *Deep Sea Res. Part I: Oceanogr. Res. Papers* **42**, 641–673 (1995).

Acknowledgements

Author contributions

P.M. conceived the study, plotted the figures, and wrote the manuscript. L.G. and T.I. helped improve and clarify the figures. C.K. provided AWI-CM1 model output and helped with data processing. J.T. provided NorESM2-LM model output and helped with data processing. J.T., J.H., T.I., C.K., M.V., S.T. and P.M.S. helped revise the manuscript, clarified the manuscript's framing, and edited the manuscript.

Competing interests

The authors declare no competing interests.

Additional information

Supplementary information The online version contains supplementary material available at https://doi.org/10.1038/s43247-024-01382-y.

Correspondence and requests for materials should be addressed to Precious Mongwe.

Peer review information *Communications Earth & Environment* thanks the anonymous reviewers for their contribution to the peer review of this work. Primary Handling Editors: José Luis Iriarte Machuca and Clare Davis. A peer review file is available.

Reprints and permissions information is available at http://www.nature.com/reprints

Publisher's note Springer Nature remains neutral with regard to jurisdictional claims in published maps and institutional affiliations.